ECS Transactions, 2 (7) 181-191 (2007)
10.1149/1.2408913, copyright The Electrochemical Society

Langmuir-Probe Characterization of an Inductively-Coupled Remote Plasma System intended for CVD and ALD

A. Boogaard, A. Y. Kovalgin, A. A. I. Aarnink, R. A. M. Wolters, J. Holleman, I. Brunets, J. Schmitz

MESA+ Research Institute, Chair of Semiconductor Components, University of Twente, P.O. Box 217, 7500 AE Enschede, The Netherlands.

We measured electron density and electron energy distribution function (EEDF) vertically through our reactor for a range of process conditions and for various gases. The EEDF of Ar plasma in the reactor could largely be described by the Maxwell-Boltzmann distribution function, but it also contained a fraction ($\sim 10^{-3}$) of electrons which were much faster (20-40 eV). At low pressures (6.8-11 μbar), the tail of fast electrons shifted to higher energies ($E_{max} \sim 50$ eV) as we measured more towards the chuck. This tail of fast electrons could be shifted to lower energies ($E_{max} \sim 30$ eV) when we increased pressure to 120 μbar or applied an external magnetic field of 9.5 μT. Addition of small amounts of N_2 (1-10%) or N_2O (5%) to Ar plasma lowered the total density of slow electrons (approx. by a factor of two) but did not change the shape of the fast-electron tail of the EEDF.
The ionization degree of Ar-plasma increased from $2.5 \cdot 10^{-4}$ to $5 \cdot 10^{-4}$ when an external magnetic field of 9.5 μT was applied.

Motivation

We built an Inductively-Coupled Remote Plasma-Enhanced Chemical Vapor Deposition (ICPECVD) system for deposition of dielectric and semi conducting layers at low substrate temperatures (~150 °C). The deposition system was designed to operate either in a chemical-vapor-deposition (CVD) or atomic-layer-deposition (ALD) mode. Both are promising techniques to deposit layers with good electrical properties at low substrate temperatures. This apparatus will be used to study the influence of physics and chemistry on the deposition process and on the electrical and physical properties of the deposited films. To do so, we need to characterize the plasma by identifying and measuring plasma species and by relating plasma characteristics to film properties.

We performed Langmuir-probe measurements in order to obtain data for the chemical modeling of our deposition processes. To model electron-stimulated reactions in plasma, one should know the reaction cross-sections, partial pressures of reactants, electron densities and electron energy distribution functions (EEDF) (1). Langmuir-probe measurements can provide us the EEDF and electron densities. These measurements allow modeling of chemical processes in plasmas, and will thus result in a better understanding and optimization of the deposition process.

Experimental

Deposition system

Downloaded 30 Jun 2009 to 130.89.112.86. Redistribution subject to ECS license or copyright; see http://www.ecsdl.org/terms_use.jsp

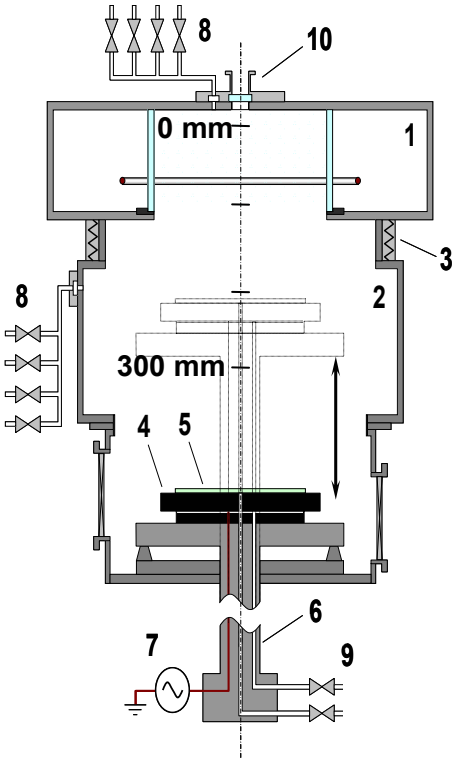

Figure 1. A schematic drawing of the remote-plasma CVD system: (1) ICP source, (2) chamber, (3) DC coil to introduce axial magnetic field, (4) chuck and susceptor, (5) wafer, (6) motor-driven arm, (7) rf-source for chuck biasing, (8) gas-inlets, (9) gas-inlet to control pressure between wafer and susceptor, and between susceptor and chuck, (10) port to introduce Langmuir probe; the gas distribution system, load lock and vacuum pumps are not shown.

Figure 1 schematically shows the system set-up. The inductive-coupled plasma source (supplied by Alcatel Micro Machining Systems; 13.56 MHz, max. electric power of 2 kW) is placed on top of the chamber (also supplied by Alcatel). Quoted electric powers are measured at the output of the rf generator (RF power products, model FR20S), and are not corrected for losses in the matching network.

The ICP-source is also equipped with external DC coils (item (3) in Fig. 1) which can induce an axial magnetic field to improve the ionization and power absorption efficiency of the plasma. The maximum magnetic field that can be applied (by setting the current through the coil) is 9.5 μT.

The wafer is placed in the load lock on a molybdenum susceptor and transferred, after a pump-down cycle, into the chamber by an automated arm, and positioned on the chuck. The chuck is situated at the bottom of this chamber. The chuck can be heated to 400 °C, but the targeted deposition temperatures should not exceed 150 °C. Temperature is controlled by a PID (proportional-integral-derivative) controller via a thermo-couple inserted into the chuck. The wafer is mechanically clamped to the chuck. Argon backing pressure of 10 mbar between the susceptor and the chuck and between the wafer and the susceptor guarantees a fairly good heat transfer between the chuck and the wafer (2). The chuck can be rf-biased and can be moved upwards into the chamber, *i.e.* towards the plasma source. Furthermore, in Figure 1 two gas inlets are shown: one on top of the plasma source and one below in the chamber. An extensive gas distribution system (not shown in the figure) will supply gases to the deposition system, eventually in a pulsed

Downloaded 30 Jun 2009 to 130.89.112.86. Redistribution subject to ECS license or copyright; see http://www.ecsdl.org/terms_use.jsp

mode. Mass flow controllers are used to control gas flows. The system is evacuated with an oil-free turbo molecular pump (Adixen ATH 1300 M, effective argon pumping speed 800 l/min) backed by a dry pump (Adixen ACP 40 G); base pressure is $5 \cdot 10^{-7}$ mbar. A set of Pfeiffer capacitance gauges is used for accurate measurement of process pressures (Pfeiffer CMR 261 and CMR 263), whereas a combined cold wall and Pirani gauge (Pfeiffer PKR 261)) measures from base pressure to atmospheric pressure.

Via the load lock, our system is connected to two thermal ALD-systems (aimed at deposition of metal barriers and dielectrics), and to an XPS and AFM/STM measurement tool. In future, these measurement tools allow us to study film compositions and morphology without vacuum break.

Plasma operation conditions

Argon was used as a carrier gas, the process pressure ranged from 6.8 to 120 μbar, while the argon flow varied between 300 and 500 sccm. Process pressure was controlled by a feedback loop to the throttle valve. A flow of 5 to 50 sccm of precursor gases nitrogen (N_2) and nitrous oxide (N_2O) was added to argon to study the influence on the EEDF and electron density in plasma. In future work, we are planning to use N_2 as a precursor for the deposition of silicon nitride and N_2O will be used to deposit silicon oxide. It is not possible to perform Langmuir-probe measurements when silane is present in the chamber, because it will form deposits on the probe. However, characterization of non-depositing mixtures is of prime importance for *e.g.* plasma-assisted ALD, which could involve such a plasma treatment as one of the steps.

Electric powers applied to plasma source ranged from 300 to 500 W.

Langmuir probe

An rf-compensated Langmuir probe (Scientific Systems SmartProbe^{TM}) was used for plasma diagnostics. The active part of the Langmuir probe is a tungsten wire of 0.19 mm in diameter and 10 mm in length. The tip is connected to an acquisition unit via a coaxial cable that is shielded from the plasma by an alumina shaft. The shaft length is 470 mm and its diameter is 9.5 mm. The shaft is mounted onto a linear drive system so that the probe can be moved in vertical direction. The drive system is placed on top of the ICP source (see Fig. 1); this enables us to measure plasma parameters vertically through the plasma-generation zone downwards to the chuck (*i.e.*, at locations between 0 and 300 mm on the axis shown in Figure 1). This drive system consists of vacuum bellows, a stepping motor and a precision ball screw arrangement. Typically, probe current is measured at bias voltages in the range from −60 to +60 V.

The problems associated with Langmuir probes in rf plasmas are well known and described in (3, 4). *Hirsch* concluded that for non-compensated probes, the apparent distribution of electrons (as measured by the probe) is a function of rf interactions in the probe sheath rather than electron energy distribution in plasma. Additionally, *Paranjpe et al.* showed that the rf voltage across the probe-plasma sheath caused a time dependent variation of the plasma potential, which very much affected the measured electron energy distribution.

The most common solution to minimize this rf distortion is provided by the manufacturers of this probe (5) and it involves increasing the probe-to-ground impedance. This ensures that the rf voltage drop mainly occurs between the probe and ground and not between the plasma and sheath.

Downloaded 30 Jun 2009 to 130.89.112.86. Redistribution subject to ECS license or copyright; see http://www.ecsdl.org/terms_use.jsp

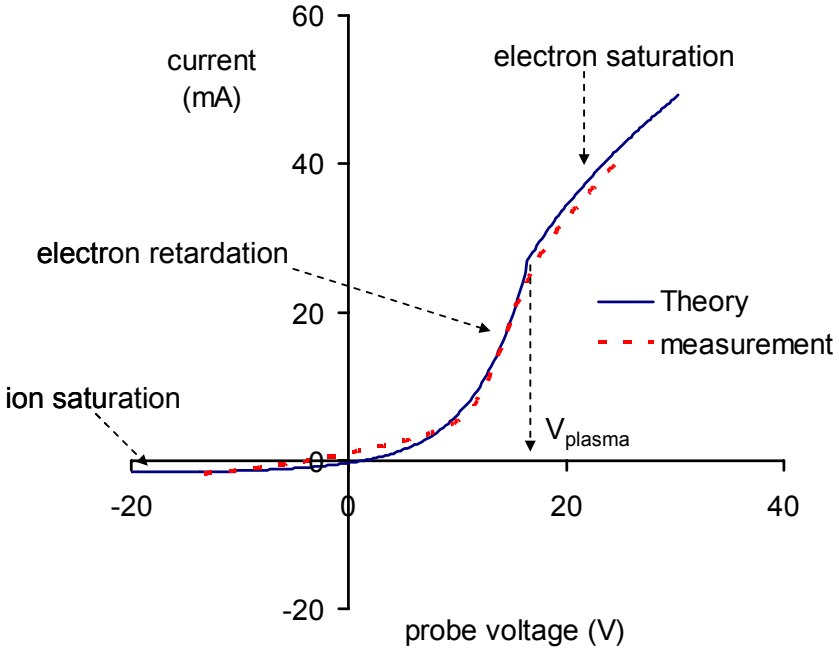

Figure 2. Typical Langmuir-probe measurement in our deposition system.
(---) Measurement in Ar plasma at 11 μbar and 300 W ICP power, probe at 80 mm;
(—) Laframboise theory fitted to those data.

A current will be collected from plasma when the probe tip is DC biased with respect to plasma, which results in an I-V curve as shown in Figure 2. Figure 2 also shows the curve as derived from Laframboise theory (6). One can see good agreement between the measured curve and theory. The plasma potential (V_p) is defined as the voltage at the transition point between the electron retarding and the electron saturation parts of the curve, *i.e.* where the second derivative is zero (V_p = 16.6 V in Figure 2). The mean electron temperature (kT_e) can be determined from the slope of the ln(I)-V curve in the region left to V_p. Next, electron density (n_e) can be calculated from the current measured at V_p using the following equation:

$$n_e = \frac{I(V_p)}{A_{probe}} \sqrt{\frac{2\pi m_e}{e^2 kT_e}} \qquad [1]$$

where A_{probe} is the surface area of the probe, m_e is the free electron mass, e is the electron charge and kT_e is the mean electron temperature in eV.

The Druyvesteyn (7) extension of the Langmuir and Mott–Smith theory (8) allows the determination of the EEDF. *Druyvesteyn* showed that the EEDF could be found from the expression,

$$N(\varepsilon) = n_e f(E) = \frac{2}{e^2 A_{probe}} \sqrt{\frac{2m_e \varepsilon}{e}} \frac{d^2 I}{dV^2} \qquad [2]$$

Downloaded 30 Jun 2009 to 130.89.112.86. Redistribution subject to ECS license or copyright; see http://www.ecsdl.org/terms_use.jsp

where $N(\varepsilon)$ is the number of electrons within energy domain $e(\varepsilon + d\varepsilon)$ eV, V is the probe voltage, ε is the probe potential with respect to the plasma potential V_p, ($\varepsilon = V_p - V$), A_{probe} is the probe surface area, d^2I/dV^2 is the second derivative of the electron current with respect to the electron energy ε, and e and m_e are the electron charge and free mass.

In this paper, the second derivative of the I-V curve is calculated numerically and averaged over 1000 values at each point on the I-V curve to reduce noise. Electron density, n_e, can also be obtained from the following integral,

$$n_e = \int_0^\infty N(\varepsilon) d\varepsilon$$

In theory, the n_e thus obtained should equal the measured n_e at V_p (see Eq. 1). In practice, these two values can differ by a factor of two.

Results and Discussion

Argon plasmas

A typical example of an EEDF in Ar plasma is shown in Figure 3. It is important to note that zero energy at the x-axis means that the probe is at plasma potential. Similarly, 50 eV corresponds to a negative probe potential of -50 V with respect to plasma potential. The y-axis shows the number of electrons within the energy domain $e(\varepsilon + d\varepsilon)$. The dotted line corresponds to the Maxwell-Boltzmann approximation of the energy distribution for a system in thermal equilibrium. The largest fraction of the electrons in our plasma is indeed in thermal equilibrium. But we also measure a fraction of electrons, which are much faster. These fast electrons can significantly influence the plasma composition, which makes them important for the chemical modeling. This is illustrated in Table I. It shows threshold energies for several electron-stimulated reactions in argon plasma, and the fraction of electrons with energies higher than these thresholds for both the Maxwell-Boltzmann and experimentally measured energy distribution. The amount of electrons which is capable of exciting argon atoms is in our case 2.5 times higher than Maxwell-Boltzmann distribution predicts. For the reactions with higher threshold energies, the difference between the Maxwell-Boltzmann distribution and experiment becomes orders of magnitude higher (see for instance the formation of double ionized argon). To successfully model chemical reactions in plasma, we certainly have to measure the EEDF, especially since it turns out to be non-Maxwellian.

Generally speaking, it should not come as a surprise that the energy distribution is non-Maxwellian. Maxwell-Boltzmann distribution is derived for equilibrium situations and a (rf) plasma is not in complete equilibrium since electrons can gain energy between collisions under the influence of the electromagnetic field. There are three theories which can describe the appearance of fast electrons in rf discharges. The first one involves elastic collisions of electrons with argon atoms at an appropriate time with respect to the phase of the electric field. If an electron makes an elastic collision, reversing its motion at the exact moment the field changes direction, then its velocity and energy would continue to increase (9-11). A second group of theories claims that the secondary electrons which are emitted from the walls and are accelerated across the positive ion sheath into the plasma act as an additional supply of electrons. If the electric field changes its direction at

Downloaded 30 Jun 2009 to 130.89.112.86. Redistribution subject to ECS license or copyright; see http://www.ecsdl.org/terms_use.jsp

the required time, this can lead to an efficient ionization (12, further references therein). Emission of electrons from surfaces can be induced by photons (photo-emission), electric field (field-induced emission) or by incoming ions (13, 14). The third theory attributes energy gain of electrons to surf riding (or wave riding) of electrons on the oscillating edge of the plasma sheath (14, 15).

At this time, it is not clear which process mainly causes the appearance of fast electrons in our system. To better understand this, a detailed analysis of these mechanisms including electromagnetic modeling of our plasma system will be carried out. Some general remarks concerning modeling can already be made below.

Although electrons with energy of 11.6 eV can ionize argon atoms to Ar^+ (see Table I), the ionization cross section is still very low (~$1 \cdot 10^{-18}$ cm^2). The ionization cross section increases rapidly for electrons with energies higher than the appearance potential until a maximum (~$2 \cdot 10^{-16}$ cm^2) is reached at energies between 40 and 200 eV (16). Furthermore, an electron in a gas may take part in several processes such as elastic scattering, excitation, ionization, recombination, and attachment. There is a certain probability for each of these processes to take place, expressed as a collision cross-section. But since each individual cross section is a probability, the overall cross-section is just the sum of the individual probabilities. For electrons in argon plasma, the total collision cross section peaks at about 14 eV (17), this happens to be the value at which our EEDF starts to deviate from the Maxwell-Boltzmann equation (see Figure 3).

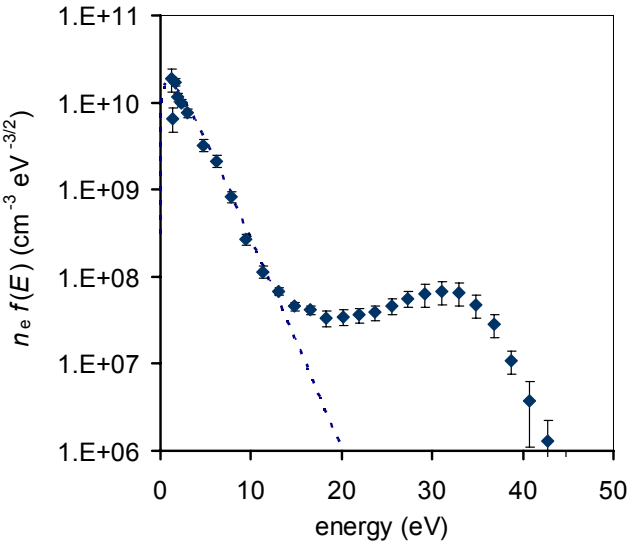

Figure 3. EEDF for argon plasma at 11 μbar, 300 W; and probe position 80 mm. The symbols represent the measurements and the dotted line represents the Maxwell-Boltzmann distribution fitted to those measurements (fitting parameters: $n_e = 5 \cdot 10^{10}$ cm^{-3} and $kT_e = 1.7$ eV).

TABLE I. Several electron-stimulated reactions in an Ar-plasma, with their appearance potentials (E_0) (18) and the fractions of electrons with energies higher than these thresholds. Fractions are calculated for the energy distribution measured in this work and the Maxwell-Boltzmann distribution (19), see Fig. 3 for fitting parameters.

		f(ε>E_0)	
Reaction	**E_O (eV)**	**Practical**	**Theory M-B**
e + Ar →Ar* + e	11.56	8.6E-03	3.2E-03
e + Ar →Ar^+ + 2e	15.76	7.1E-03	3.5E-04
e + Ar →Ar^{2+} + 3e	27.61	3.5E-03	4.0E-07

Downloaded 30 Jun 2009 to 130.89.112.86. Redistribution subject to ECS license or copyright; see http://www.ecsdl.org/terms_use.jsp

Figure 4 shows the electron energy distribution at several pressures (7, 36 and 120 µbar) and at several probe locations in the system (*i.e.*, 80 mm, 180 mm and 240 mm). Comparing the energy distributions of the slow electrons at different pressures, one can see that the mean electron energy decreases with increasing pressure. This can be explained by the shorter mean free path at higher pressures reducing the acceleration time between two collisions. Furthermore, the peak corresponding to fast electrons shifts to lower energies at higher pressures. This could also be caused by the decreased mean free path by which the fast electrons can pick up less energy from the electric field.

With respect to the EEDF at 6.8 µbar (see Fig.4a), it appears that the tail of fast electrons shifts to higher energies with an increasing distance from the ICP-source: compare the rhombic symbols (measured at 80 mm) with the triangles (measured on 180 mm) and the circular symbols (240 mm). Please note that Figure 6a shows the same behavior for a higher pressure of 11 µbar. This observed effect is quite opposite of what is desired for a remote plasma system, namely a minimization of the substrate bombardment with fast electrons. At higher pressures this shift to higher energies decreases (Fig. 4b), or disappears (Fig. 4c).

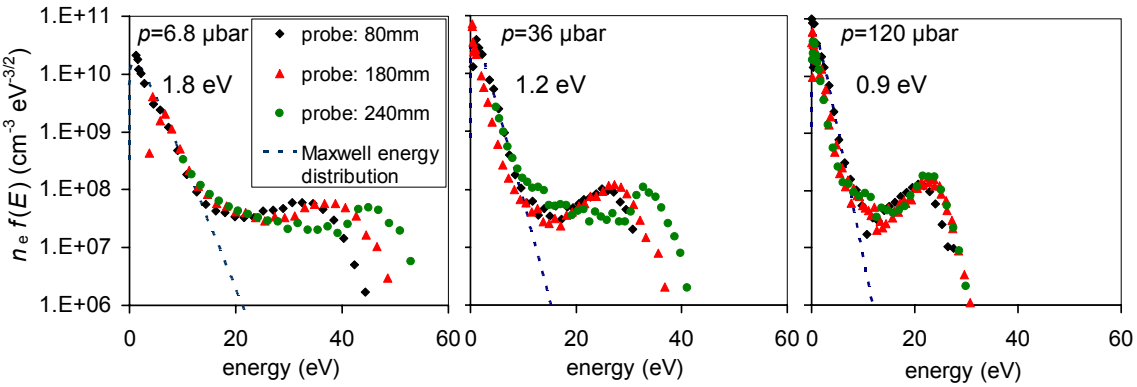

Figure 4. EEDFs for Ar plasmas at several pressures and probe positions. ICP power: 300 W. The symbols represent the measurements and the dotted lines represent the Maxwell-Boltzmann distribution fitted to those measurements. Mean electron energies used for the Maxwell-Boltzmann distributions are listed in the figures.

External axial magnetic field. The ionization degree of the plasma can be increased by applying an external axial magnetic field. Due to the Lorentz force, the length of the electron trajectory is increased, which results in more collisions and better ionization efficiency (20). The influence of a magnetic field is shown in Figure 5. In these experiments we measured the electron density at several positions in the system ranging from 0 mm to 300 mm along the axis shown in Fig.1. The highest electron density can be seen at the rf coil position, with a maximum electron density of $n_e = 7 \cdot 10^{10}$ cm^{-3} without an external magnetic field. The density of argon atoms at 11 µbar can be calculated by Avogadro's law to be $n_{Ar} = 2.75 \cdot 10^{14}$ cm^{-3} (21); assuming that the ion density (n_i) roughly equals the electron density, the maximum ionization degree (n_i/n_{Ar}) of this plasma is $2.5 \cdot 10^{-4}$ at these conditions. Then, a gradual decrease in electron density can be seen with increasing distance from the rf coil towards the chuck. This decrease is caused by capture of electrons on the reactor walls. Electron density increases as the intensity of the axial magnetic field is increased, which is in line with theory. Measurements show that the

Downloaded 30 Jun 2009 to 130.89.112.86. Redistribution subject to ECS license or copyright; see http://www.ecsdl.org/terms_use.jsp

electron density increases from $n_e = 7 \cdot 10^{10}$ cm^{-3} without magnetic field to $n_e = 1.4 \cdot 10^{11}$ cm^{-3} with an external magnetic field of 9.5 μT.

The EEDF is also affected by the external magnetic field; this is shown Figure 6. The EEDFs in Figure 6a were measured without an external magnetic field at three positions in the chamber. Figures 6b and 6c show the energy distributions at the same positions but in the presence of a magnetic field. By increasing the field, the distributions shift to lower energies. This can be explained as follows. Electron trajectories are deviated by a Lorentz force, which is proportional to the product of magnetic field intensity and electron velocity. So, fast electrons are influenced more effectively in such plasma than slow electrons. This will result in more collisions for fast electrons.

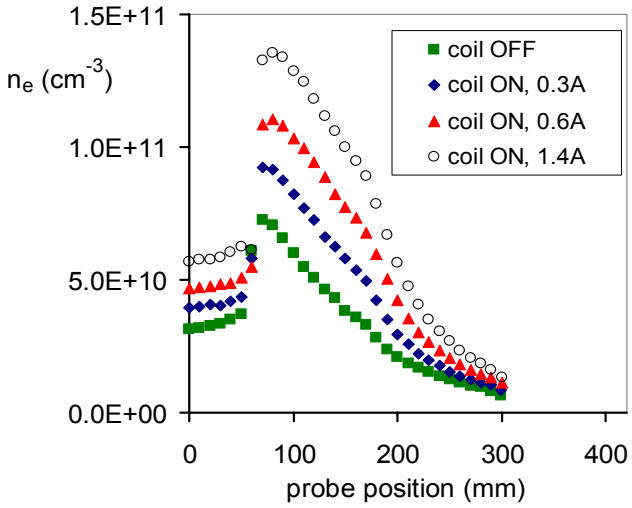

Figure 5. Electron densities in Ar plasma (11 μbar, 300 W ICP power) versus probe locations in the system, plotted for several magnetic field strengths. (■) $B = 0$ T; (♦) $B = 2$ μT; (▲) $B = 4$ μT;(○) $B = 9.5$ μT.

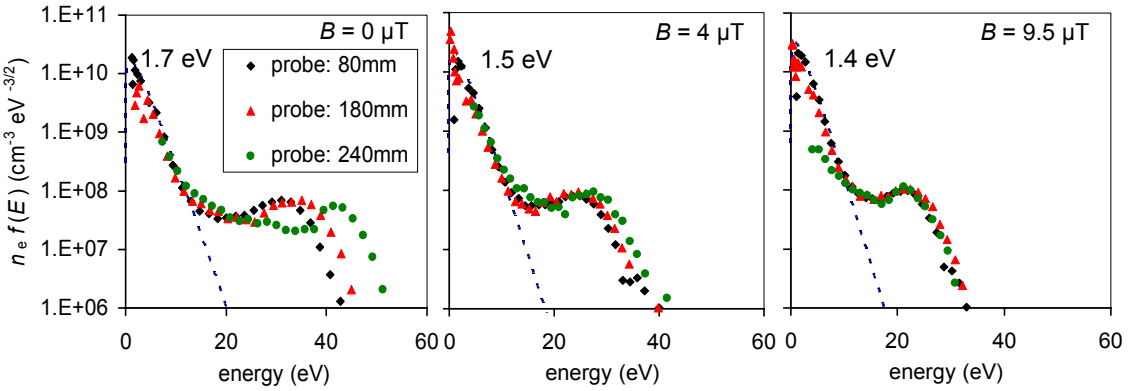

(a) (b) (c)

Figure 6. EEDFs for Ar plasmas (11 μbar, 300 W ICP power) for several magnetic field intensities and probe positions. The symbols correspond to measurements and the dotted line represents the Maxwell-Boltzmann distribution fitted to those measurements. Mean electron energies used for Maxwell-Boltzmann distributions are listed in the figures.

Downloaded 30 Jun 2009 to 130.89.112.86. Redistribution subject to ECS license or copyright; see http://www.ecsdl.org/terms_use.jsp

Ar-N_2 and Ar-N_2O plasmas

In this section we demonstrate the influence of nitrogen and nitrous oxide on the EEDF and electron density. Figure 7 shows the results of these experiments. Small amounts of N_2 added to Ar plasma decreases the total number of slow electrons (see Fig. 7a), however the tail of fast electrons remains nearly the same. The same holds when small amounts of N_2O are introduced instead of N_2 (see Fig. 7b). This is an important result for chemical modeling. However, the EEDF looks different for pure nitrogen plasma (see plus symbols in Fig. 7a).

In our future work, we aim to make a correlation between the Langmuir-probe characterization and Optical Emission Spectroscopy (OES) measurements. OES can be used to obtain *e.g.* mean electron energies (22, 23) and concentrations of certain particles in plasma (24, 25, 26). OES is one of the few *in situ* techniques to investigate the influence of silane on the parameters of Ar and/or Ar-N_2/N_2O plasmas.

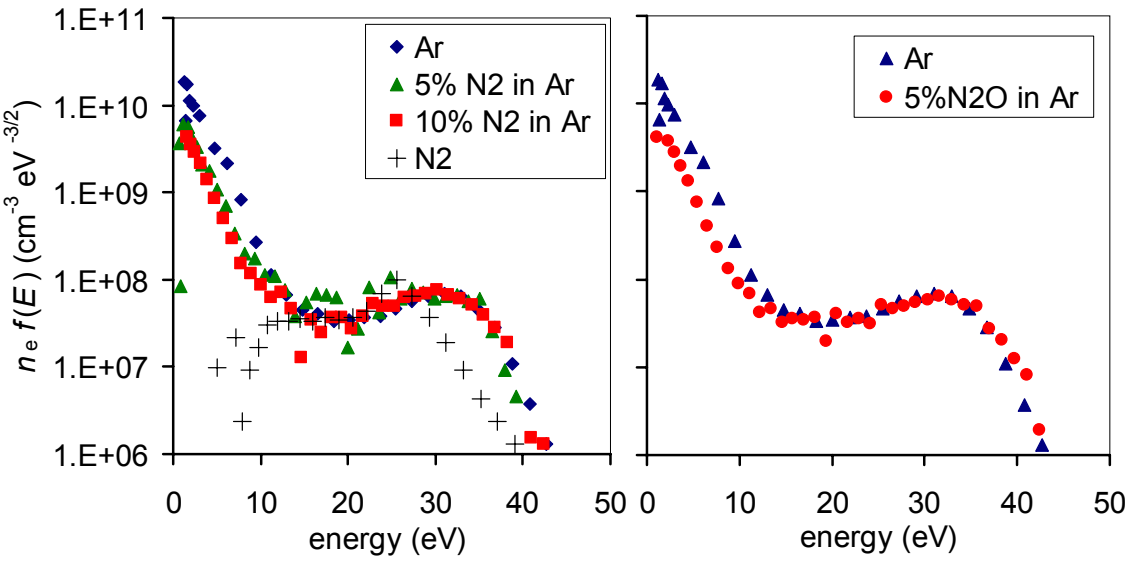

Figure 7. Electron Energy distribution functions for (a) Ar/N_2 plasma and (b) Ar/N_2O plasma measured at different probe positions (ICP power: 300 W; p = 11 μbar).

Conclusions

We presented our results on a series of Langmuir-probe measurements, which were carried out for characterization of a High-Density Inductively-Coupled Remote Plasma-Enhanced Chemical Vapor Deposition (remote ICPECVD) system. We measured electron densities and electron energy distribution functions in different plasmas, which are to be used to model plasma processes and deposition kinetics. Plasma characteristics were measured for Ar plasmas at several probe locations in the chamber.

Measured EEDFs can be divided in two parts: a large part of 'slow' electrons which exhibit Maxwell-Boltzmann energy distributions and a smaller part (~ 10^{-3}) of 'fast' electrons in the energy range of 20 to 40 eV, deviating from Maxwell-Boltzmann distribution.

Mean electron energy of the slow electrons decreases with increasing gas pressure; from kT_e = 1.8 eV at 6.7 μbar to kT_e = 0.9 eV at 120 μbar. The fast electron tail shifts to lower energies when the pressure is increased (*i.e.*, from 33 eV at 6.7 μbar to 22 eV at

Downloaded 30 Jun 2009 to 130.89.112.86. Redistribution subject to ECS license or copyright; see http://www.ecsdl.org/terms_use.jsp

120 μbar). Similar effects can be observed when an external axial magnetic field is applied to the plasma; kT_e of slow electrons decreases from 1.7 eV to 1.4 eV (at 11 μbar) when a magnetic field of 9.5 μT is applied, and the fast electron tail shifts from 32 eV to 22 eV.

In a low pressure regime (*i.e.*, p < 11 μbar), the tail of fast electrons shifts to higher energies closer to the chuck. Apparently, electrons make fewer collisions at these low pressures and can gain more energy between collisions from the electric field.

Addition of small amounts of N_2 (5-10%) or N_2O (5%) to the Ar plasma did not change the shape of the fast-electron tail of the EEDF, but decreased the densities of slow electrons by approximately a factor of two.

Acknowledgments

The authors would like to thank Alcatel for supplying the ICP source, deposition chamber and Langmuir probe. We would also like to thank B. Andrieu, H. Beaujon, N. Launay, L. Popin, and M. Puech from Alcatel Micro Machining Systems, Annecy, France for their fruitful comments and cooperation.

The ICP system was designed and realized in close cooperation with 'Techno Centre for Education and Research' of University of Twente.

This work (project number STW-TEL 6358) is supported by the Dutch Technology Foundation (STW).

References

1. I. Haller, *J. Vac. Sci. Technol. A*, **1**, 1376 (1983).
2. A. M. van Graven and R. A. M. Wolters, *Microelectron. Eng.*, **50**, p. 495 (2000).
3. E. H. Hirsch, *Int. J. Electron.*, **19**, 537 (1965).
4. A. P. Paranjpe, J. P. McVittie and S. A. Self, *Journal of Applied Physics*, **67**, 6718 (1990).
5. R. R. J. Gagné and A. Cantin, *J. Appl. Phys.*, **43**, 2639 (1972).
6. R. M. Clements, *J. Vac. Sci. Technol.*, **15**, 193 (1978).
7. M. J. Druyvesteyn, *Z. Phys. A Hadron Nucl.*, **64**, 781 (1930).
8. I. Langmuir and H. Mott-Smith, *Gen. Elect. Rev.* **27** 449 (1924).
9. A. D. MacDonald and S. J. Tetenbaum, in *Gaseous Electronics vol. 1: electrical discharges*, M. E. Hirsch and H. J. Oskam, Editors, p.173, Academic Press, New York and London (1978).
10. H. R. Koenig and L. I. Maissel, *IBM J. Res. Dev.*, **44,** 106 (2000).
11. L. I. Maissel, in *Handbook of thin film technology*, L. I. Maissel and R. Glang, Editors, p. 4-32, McGraw-Hill, New York (1970).
12. G. N. Jackson, *Thin Solid Films*, **5**, 209 (1970).
13. T. Makabe and I. Petrovic, *Plasma Electronics: Applications in Microelectronic Device Fabrication*, p.127-134, Taylor & Francis, Boca Raton (2006).
14. A. J. van Roosmalen, J. A. G. Baggerman and S. J. H. Brader, *Dry Etching for VLSI*, p. 62, Plenum Press, New York and London (1991).
15. J. H. Keller and W. B. Pennebaker, *IBM J. Res. Dev.*, **23,** 3 (1979).
16. G. G. Raju, *Gaseous electronics: theory and practice*, p. 109, Taylor & Francis, Boca Raton (2006).
17. G. G. Raju, *Gaseous electronics: theory and practice*, p. 97, Taylor & Francis, Boca Raton (2006).

Downloaded 30 Jun 2009 to 130.89.112.86. Redistribution subject to ECS license or copyright; see http://www.ecsdl.org/terms_use.jsp

18. B. Chapman, *Glow discharge processes*, p. 119, Wiley, New York (1980).
19. B. Chapman, *Glow discharge processes*, p. 118, Wiley, New York (1980).
20. A. J. van Roosmalen, J. A. G. Baggerman and S. J. H. Brader, *Dry Etching for VLSI*, p. 92, Plenum Press, New York and London (1991).
21. B. Chapman, *Glow discharge processes*, p. 7, Wiley, New York (1980).
22. I. M. Podgornyi, *Topics in Plasma Diagnostics*, p. 39, Plenum Press, New York (1971).
23. J. Felts and E. Lopata, *J. Vac. Sci. Technol. A*, **6**, p. 2051 (1988).
24. R. A. Gottscho and V. M. Donnelly, *J. Appl. Phys.*, **56**, 245 (1984).
25. W. M. M. Kessels, M. C. M. van de Sanden, D. C. Schram, *J. Vac. Sci. Technol. A*, **18**, 2153 (2000).
26. A. J. van Roosmalen, J. A. G. Baggerman and S. J. H. Brader, *Dry Etching for VLSI*, p. 141, Plenum Press, New York and London (1991).

Downloaded 30 Jun 2009 to 130.89.112.86. Redistribution subject to ECS license or copyright; see http://www.ecsdl.org/terms_use.jsp